Amalgamation and Characterization of Copper Nanoparticles Alleviated With Stachytarpheta Cayennensis and Its Anti-cancer Activity in Both in Vitro and in Vivo Animal Model

Vidya Devanathadesikan Seshadri (vidya205@gmail.com)
Department of Pharmacology & Toxicology,College of Pharmacy, Prince Sattam Bin Abdul Aziz University,Al –Kharj, Kingdom of Saudi Arabia.

Original Research Full Papers

Keywords: Stachytarpheta cayennensis, copper nanoparticles, skin cancer, A375 cells, NF-κB, iNOS, COX-2

DOI: https://doi.org/10.21203/rs.3.rs-161215/v1

Abstract

Melanoma is an extremely malignant skin cancer with a probability of metastasis and accountable for the mainstream skin associated mortality. In the present study, we described the novel usage of *Stachytarpheta cayennensis* mediated copper nanoparticles and its anti-cancer activity in both *in vitro* and *in vivo* model of skin cancer. The synthesis of Cu-NPs was confirmed using UV-absorbance peak values ranging from 325-345 nm. The size of the nanoparticles was around 90nm, as deduced by the dynamic light scattering study.Furthermore, transmission electron microscopy (TEM) established that the morphology of the copper particles. Cytotoxicity of Cu-NPs of *Stachytarpheta cayennensis* illustrates the toxicity level of *Stachytarpheta cayennensis*. Also, the anti-cancer potential of Cu-NPs was evaluated in A375 cells. In experimental animals, body biochemical parameters like SOD, CAT, GSH were diminished in DMBA induced animals while Cu-NPs treatment raised the levels of the aforementioned enzymatic antioxidants compared to the control animals. Additionally, cytotoxicity assay, mitochondrial membrane potential (MMP), cell adhesion analysis, and the estimation of reactive oxygen species (ROS) in the presence of Cu-NPs was evaluated by standard protocols. The present study's outcomes confirm the defensive and valuable effects of copper loaded *Stachytarpheta cayennensis* against DMBA induced skin melanoma, animal model.

1. Introduction

Melanoma is the malignancy of melanocytes which exist as single cells inside the basal layer of cuticles. Melanoma is an extremely malignant skin cancer with a probability of metastasis and accountable for the mainstream skin associated mortality. The 5-year existence of melanoma is about 10% (Miller et al., 2020). To date, melanoma is one of the world's critical medical challenges. The unsuccessful therapy is complemented with chemotherapy, which might lead to toxic and side effects on individuals. Also, few familiar drugs, such as metformin, were too used for melanoma cancer treatment in the clinic. In current years, the speedy propagation of nanotechnology and the nano-related treatment approach could offer a novel idea for treating melanoma cancer (Hong Feng et al. 2019). Nanoparticles (NPs) are progressively contributing to the opportunity of their usage in the expansion of new healing methods in the arena of cancer. Nanoscale particles are the emerging sources of useful medications due to their high exterior to capacity ratio and improved reactive surface area. The growing anticancer candidates nano-patterned from decorative metals like copper, silver, and gold are increasingly recognized (Li et al., 2020; Zottel et al. 2019). Since copper is inexpensive than gold and silver, the expansion of copper-related NP's as curative is preferred for developing therapeutics. The biomedical applications of copper nanoparticles were already proved earlier (Akintelu et al., 2020).

Though there are abundant findings on the anticancer outcome of copper oxide nanoparticles, there is inadequate research available on the anticancer effectiveness of metallic copper nanoparticles (Wang et al. 2012; Siddiqui et al. 2013; Sun et al. 2012; Wang et al. 2013; Laha et al. 2013). The primary objective of choosing Cu-NPs is to get an alleviated arrangement of NP's at ambiguous temperatures since copper is generally corroded under these circumstances. A further report articulates a new technique of

synthesizing Cu-NP, which continued to be stable at ambient temperatures (Yaqub et al., 2020). The bactericidal action of the elements on Gram-negative and Gram-positive bacteria was much effective than that of the Cu-NPs synthesized using additional methods (Sanchez-Lopez et al., 2020; uparelia et al. 2008; Yoon et al. 2007; Raffi et al. 2010). Nanoparticle manufacture's physical and chemical procedures are characteristically luxurious and necessitate harmful chemicals, while the green synthesis method is environmentally friendly and less costly. Plants form the most discovered collection of living organisms available for the green synthesis of nanoparticles (Silva et al. 2015). Herbal harvests can also play a central role in covering adaptable groups, avoiding the necessity for ligand interchange preceding to living or organic aspects. However, greener or biogenic approaches do not assure nanomaterials' production with enhanced or flat undistinguishable possessions than those fashioned by outdated procedures (Metz et al. 2015).

Earlier reports suggest that wildflowers, the unsolicited plants in the farming setups, can be employed for synthesizing nanoparticles (Francois et al. 2019). *Stachytarpheta cayennensis* is a ligneous weed with 0.5–1m height. This plant's leaves are used in traditional medication to improve digestion and as an antipyretic to cure chronic liver disorders, shafts, coughing and ache in bone, and high urine passage and excess sweating (Schapoval et al. 1998). It was already proved that the *Stachytarpheta cayennensis* has potent antimicrobial, antispasmodic, anti-inflammatory, and anti-ulcerogenic activities (Okoye et al., 2010; Panido et al., 2006). *Stachytarpheta cayennensis* extracts have proven useful as an antimicrobial, antispasmodic, and anti-diabetic agent. Phytochemical characterization exposed the occurrence of carbohydrates, flavonoids, terpenoids, and saponins (Adebajo et al. 2007; Okoye et al. 2010) in the plant extract. In the present study, we describe the novel usage of *Stachytarpheta cayennensis* plant extract for copper nanoparticle preparation. Additionally, in-vitro antioxidant and anticancer trials show the efficient pharmacological usage of such nanoparticles.

2. Material And Methods

2.1 Cell lines and Chemicals

Dulbecco's Modified Eagle's Medium (DMEM), trypsin-EDTA, Human melanoma cells (A375), dimethyl sulfoxide (DMSO), antibiotics such as penicillin or streptomycin, DMBA (7,12 dimethylbenzanthracene), fetal bovine serum (FBS), was procured from Sigma-Aldrich (St. Louis, USA). Acridine Orange (AO), ethidium bromide (EB), and 2',7'-dichlorofluorescein diacetate (DCFH-DA) were acquired from Chem Cruz Biochemicals, (California, USA). All laboratory reagents and chemicals utilized in the present study were of analytical grade.

2.2 Plant and Extract Composition

The test plants of *Stachytarpheta cayennensis* were obtained from Eziobodo communal, Owerri West, Nigeria (L.G.A of Imo state). The plant leaves were sliced into small pieces and cleaned under running tap water to remove sand particles. Leaves were then dehydrated in a room for a month and crushed into powder using a crushing machine. The crushed sample was then deposited in sealed decanters until

used for the study (Iwu et al. 2018). Aqueous plant extracts were prepared by sweltering 10gm of biological material in 200mL of de-ionized liquid for 10min at 80˚C. The extract was sieved via Whatman No. 1 filter paper to eliminate particulate matter. The purified solution was then deposited at 4˚C for supplementary usage for one week owing to the steady loss of plant extract during continued storing (Meva et al. 2016).

2.3 Synthesis of copper nanoparticles

Freshly prepared 5mM copper acetate solution of about 190ml was mixed with 10ml of the plant extract under continuous stirring. Copper nanoparticles (CuNPs) formed after the reaction was recovered through centrifugation, lyophilized, and deposited at 4°C for succeeding studies. Lyophilized material was dissolved in distilled water with brief sonication and taken for further studies (Ria Mukhopadhyay et al. 2018).

2.4 Characterization of synthesized copper nanoparticles

2.4.1 Ultraviolet-Visible Spectroscopy

The synthesized copper nanoparticles were characterized using a UV-visible spectrophotometer functioning at 1nm determination with an ophthalmic measurement of 10mm. Absorptions were determined after 24h of nanoparticle development recovered by centrifugation at 5000rpm within one hour. UV-Vis examination of the response combination was carried out for 300 seconds (Francois et al. 2019).

2.4.2 Dynamic light scattering

To normalize the particle magnitude or dimension of the synthesized copper nanoparticles, they were analyzed using dynamic light scattering (Shi et al., 2014). In this method, 0.01gm of polymer precipitation included 12mmol silver nitrate in 20ml purified solutions.

2.4.3 FTIR spectroscopy

FTIR examination was carried out to comprehend probable relations between the active component of plant extracts and the copper ions. The FTIR range of lyophilized plant extract of *Stachytarpheta cayennensis* and copper nanoparticles was documented on a potassium bromide pellet in the FTIR spectrophotometer (Bruker, INVENIO, Tensor-37) over a particular frequency of wave range from 4000 – 400 cm^{-1} (Ria Mukhopadhyay et al. 2018).

2.4.4 Transmission electron microscopy

The structure of the copper nanoparticles was resolved by transmission electron microscopy (JEOL JEM 1200, Czech Republic). From 1mg/ml suspension of copper nanoparticles, a drop was positioned on a 300-lattice carbon covered copper electron microscope grid and then systematically air-dried for 10hr. The dehydrated sample was then observed at 120 kV underneath a conventional electron microscope (Ria Mukhopadhyay et al. 2018).

2.5 *In vitro* assays

2.5.1 MTT cytotoxicity assay

Cell toxicity by Cu-NP was scrutinized using the typical MTT (3-(4,5- dimethylthiazol-2-yl)-2, 5-diphenyl-tetrazolium bromide, Sigma) assay (Mosmann 1983). The principle of MTT assay is that the mitochondrial dehydrogenase enzyme of viable cells breakdown the tetrazolium salts present in the membrane, which reacts with the MTT dye, resulting in the formation of purple formazan crystals, that is soluble in isopropanol or DMSO. The absorbance of these crystals can be measured at 580nm. The progressed inhibition of Cu-NP treated cells was articulated as the proportion inhibitory concentration (IC) compared to the unprocessed control cells. For the experiment, 4×10^4 cells per well were seeded in 24 well microtiter plates, mixed with MTT dye at a final concentration of 0.5 mg/ml. The cells were incubated for 3-4hr in the dark condition at room temperature. The MTT solution was then discarded from the plated, supplemented with acidic isopropanol (Merck, USA), and incubated for further 10min to solubilize the formazan crystals. The absorbance was measured using a Shimadzu, UV-1900i instrument at 580nm.

2.5.2 Cell adhesion assay

Copper nanoparticles were prepared by succeeding amalgamation with trypsin. Then *Stachytarpheta cayennensis* were distributed to microtiter plates. Cu-NPs was disconnected at a different time, and wells were washed with phosphate buffer, and the resultant solution was eliminated excitedly in contrast to committed cells. Cells steadfast beneath the microtiter plate were stained with crystal violet dye and paraformaldehyde, further supplemented with the Cu-NPs plates and incubated for 20min. After that discoloration, excess crystal violet dye was cleaned by phosphate-buffered saline solution. Crystal violet binds to the intracellular proteins. The amount of crystal violet bound to the proteins was proportional to the number of cells in the dishes. The crystal violet dye was extracted using isopropanol, and the purple color was measured at 540nm in the reader (Ruan et al. 2012).

2.5.3 Estimation of intracellular ROS

The reactive oxygen species produced inside the cell was estimated by the method as reported earlier (Gunaseelan et al. 2017) using DCFDA (2, 7-dichlorofluorescein diacetate, Thermo Fisher Scientific, USA) dye. Cu-NPs at 5µg/mL and 10µg/mL was added to the microtiter plate. After one day of incubation, the cells were exposed to Cu-NPs for 4-5hr. Following this, the plates were washed three times by saline with phosphate as a buffering agent and incubated with DCFDA dye (20µM) for about 45mins at room temperature. The cells were then washed with 200µl of buffered saline phosphate, and the dye uptake was recorded in a multimode reader (Sigma, USA) at wavelengths of 540 and 490nm excitation/emission, respectively. The confirmation of the ROS generation was analyzed through a fluorescence microscope (Sigma, USA).

2.5.4 Mitochondrial membrane potential

This method is interesting to inspect the transmembrane efficacy, which employs the probe 5,5',6,6'-tetrachloro-1,1',3,3'-tetraethylbenzimidazolcarbocyanine iodide (Srilatha Sakamuru et al. 2016). Cells were treated with Cu-NPs followed by trypsin and washed with phosphate buffer saline several times. Then Cu-NPs treated cells were incubated with a membrane dye, JC-1 (10μM) for around 15min at room temperature, and washed with phosphate buffer saline. The cells were excited with green and red wavelengths using Phase Contrast fluorescence microscope (Thermo Fischer Scientific, USA).

2.5.5 Acridine Orange/Ethidium bromide staining

The EtBr/AO staining helps detect the difference between dead and viable cells under the fluorescence microscope. Also, it differentiates the apoptotic DNA damage and the condensed chromatin of apoptotic cells. AO can easily penetrate viable and dead cells, and EtBr interacts with DNA, which appears as orange, red spots. For dual staining, cells were seeded into 12-well plates and treated with Cu-NP's at 5μg/mL and 10μg/ml for approximately 24hr. Then the cells were washed with (Deborah Ribble et al. 2005). After staining with acridine orange (100μg/ml) and ethidium bromide (100μg/ml) phosphate buffer saline (200μl), the cells were again washed with buffered saline water to remove the unbound dyes. Then we inspected discoloration implications utilizing a fluorescence microscope (Cell imagery systems, Sigma Aldrich, USA).

2.6 *In vivo* experiments

2.6.1 Experimental design

For animal studies, Swiss male albino mice (18-22gm) were utilized in the present study. The animals were obtained from the Shanghai Animal Center (Shanghai Laboratory, China). All the animals used in this study were recognized with standard attention in compliance with animal care strategies by the National Institutes of Health, United States. The study was approved by the Institutional Animal Ethics committee, North Sichuan Medical College, Nanchong, 637100, Sichuan, China (IAEC No:2019-15). All mice were divided into four groups of 6 mice (n = 6 each). The Group I mice were considered control and administered normal diet, and acetone alone was used during experimentation. Group II mice were treated with 25μg of DMBA in 100μL acetone through the dorsal region injection. Groups III mice were treated with DMBA and CuNPs at 10mg/kg b.w in 1% DMSO. Group IV mice were administered with CuNPs (10mg/kg b.w) alone. Oral administration of CuNps (10mg/kg bw) was carried out thrice a week, early from the week of commencement DMBA treatment till 25 weeks. At the end of the 25 weeks, biochemical and molecular level studies were carried out, and skin tissue was dichotomized out control and investigational animals.

2.6.2 Assessment of antioxidant levels in the serum of experimental animals

The level of antioxidants in the serum of control and experimental animals were analyzed by standard methods. Primarily, a blank trial containing 2mL reagent and 1mL distilled water were utilized. The reaction was initiated by adding up of 10% trichloroacetic acid and thiobarbituric acid, TBA (0.375%) to

0.025 normality HCl, and mixed gently till TBA entirely liquefied (Rahmat et al. 2017). The serum of 0.5mL was mixed with 0.5mL sterile water in a 1.5mL centrifuge tube. The reaction mixture was added to each sample, incubated at 37°C in a water bath for 10 min, and centrifuged at 2000×g for 20 minutes. The optical density values were recorded at 540nm, and the supernatant was transferred to new tubes. Likewise, the antioxidative molecules were estimated by the malondialdehyde standard index. Superoxide dismutase enzyme action was performed according to the previously described method (Sun et al. 2012). The catalase enzyme action was studied by spectrophotometry, followed by the hydrogen peroxide deprivation speed per minute, according to the standard method described earlier (Goth 1991). Other additional biochemical assays like GSH, and GPx were determined by the standard protocol (Rahmat et al. 2017).

2.6.3 Assessment for pro-inflammatory markers and interleukin levels

The level of pro-inflammatory markers, i.e., IL-6, IL-1β, and TNF-α in the serum of both control and experimental animals, were analyzed by enzyme-linked immunosorbent assay (ELISA) kits (Thermo Fischer Scientific, USA). All the experimental procedures were followed according to the user manual instructions.

2.6.4 RT-PCR analysis

The total RNA was extracted from the skin tissues of both control and Cu-NP-treated animals with the help of Trizol RNA extracting kit (Santacruz Biotech, USA) by the manufacturer's protocols. The extracted RNA from the experimental animals was utilized to construct the cDNA using the a commercial RT-PCR assay kit (Santacruz Biotech, USA). The primers used for NF-κB forward: 5'-GTGGTGCCTCACTGCTAACT-3' and reverse: 5'-GGATGCACTTCAGCTTCTGT-3'; COX-2 forward: 5'-ACACACTCTATCACTGGCACC-3' and reverse: 5'-TTCAGGGAGAAGCGTTTGC-3'; iNOS forward: 5'-CAGCTGGGCTGTACAAACCTT-3' and reverse: 5'-CATTGGAAGTGAAGCGGTTCG-3'. The reaction was sustained with initial denaturation for the 30s at 95°C, subsequently 40 PCR cycles with 5s of denaturation at 95°C, annealing for 30s at 60°C and extension for 15s at 95°C. The whole test was executed in triplicate for precise measurements, and the obtained results were expressed as relative mRNA expression (fold change).

2.6.5 Histopathology

For histopathological investigations, the formalin embedded skin tissue segments from both control and experimental animals were fixed in paraffin, subdivided, and then located onto miniature infinitesimal slides followed by standard histopathological measures. The skin tissue sections were stained with hematoxylin and eosin (H&E staining) and imaged using light microscopy (Attalla and El-Kott 2015).

2.7 Statistical analysis

The experimentations were carried out in triplicates, and the results were represented as mean ± standard deviation (SD). Values with $p < 0.05$ were considered statistically significant.

3. Results

3.1 Depiction of UV-Visible Spectroscopy

The reduction of copper loaded *Stachytarpheta cayennensis* extract was confirmed by UV-Vis Spectrophotometer. The UV visible spectra of Cu-NP's have been displayed in Fig. 1. The UV-VIS absorption of Cu-NP's was the highest around 370nm, which is equivalent to that of copper nanoparticles. Consequent to development, the color was temporarily biased of the excitation state of surface plasmon situation in the Cu-NPs. The decrease of copper was examined through UV-VIS Spectrophotometer. Absorption curves of Cu-NP's have a range around 300nm, and enlargement of peak specifies that the vital essentials are disconnected. The steadiness also ranges the surface plasmon captivation, which relies on the volume of the metal nanoparticles and the dielectric constant (Melvin et al. 2009). *Stachytarpheta cayennensis* and copper acetate changed the shade of the Cu-NPs. The highest absorption at 370nm was tentative, which denotes the entire corrosion of copper ions. The UV-Vis accessory range of Cu-NPs is recognized with a penetrating optical density at 370nm, which designates a projected consistent arrangement of the nanoparticles.

3.2 Dynamic light scattering analysis

Dynamic light scattering (DLS) is a technique used to measure the hydrodynamic size of the synthesized nanoparticles. Figure 2 shows Cu-NP's particle proportions in the nanosheets. It was established through subsequent tentative statistics that copper loaded *Stachytarpheta cayennensis* extract had a size of 100nm. The highest percentage of copper loaded Stachytarpheta existing in the solution was of 52.50nm.

3.3 Representation by Fourier Transform Infrared Spectroscopy for NP's

FTIR examination is an excellent and approved technique to differentiate the biological compounds that remained accountable for breaking down metal ions into Cu-NPs in the presence of *Stachytarpheta cayennensis*. (Fig. 3). The phyto-component in the extracts was responsible for the configuration of the variability of nanoparticles. The FTIR array of *Stachytarpheta cayennensis* demonstrated recurrent combined peaks from 3266cm^{-1} to 660cm^{-1}. Figure 3 exhibits the descriptive FTIR range achieved from *Stachytarpheta cayennensis*. The incidence commences from 3266cm^{-1}, and points characterize the OH extending tremor and the presence of amino acids along with sugar molecules. The occurrences are 2909cm^{-1} peaks suggest the hydrogen and carbon covering particularly, lipids. The manifestation of peaks from 1612cm^{-1} peaks in the amide group C = O denotes the protein fragments. Then the existence range of 1318 cm^{-1} peak symbolizes sulfur multiplexes. The prevalence of Cu-NP's 27cm^{-1} peaks validates the carbon-nitrogen in the amino acids.

3.4 Cu-NPs absorption examined by transmission electron microscope

We assessed the morphology and the size range of nanoparticles through transmission electron microscopy in the current study. TEM images of synthesized Cu-NP's are illustrated in Fig. 4. The TEM images of Cu-NPs revealed that they possessed irregular and partially oval-shaped structures with an average size ranging from 20-100nm.

3.5 Cytotoxicity outcomes of *Stachytarpheta cayennensis* Cu-NPs

The cytotoxicity effect of Cu-NPs in A375 cells was assessed by MTT assay. Figure 5 discloses the cell probability assay for normal A375 cells, which were primarily examined in a concentration-dependent manner (1, 2.5, 5, 7.5, and 10µg/ml), and the viability was normalized between 5 to 10µg/ml. Therefore, A375 cells were exposed to *Stachytarpheta cayennensis* Cu-NPs for about 24hr. Accordingly, the MTT outcomes documented the concentration needed for Cu-NP's cytotoxicity, as displayed in Fig. 5. The amount of mitochondrial damage investigated after 24hr exposure to two different concentrations of Cu-NP's, i.e., 5, 7.5 mg/ml, was 95% and 85%.

3.6 Cell adhesion evaluation using *Stachytarpheta cayennensis* copper nanoparticles

Figure 6 demonstrates the examination of adhesive cells in control, *Stachytarpheta cayennensis* copper nanoparticles treated, and other experimental groups. The cells were evaluated for 24hr to get improved adherent consequences. Both control, *Stachytarpheta cayennensis* copper nanoparticles (5&7.5µg/ml) showed reasonable adherent cells compared to other groups. While in gestation time, intermission of 24hr control and *Stachytarpheta cayennensis* clusters exemplifies attached cells. Eventually, our fallouts display the optimistic outcome of *Stachytarpheta cayennensis* in adhesion assay.

3.7 Stachytarpheta cayennensis on intracellular ROS production

The A375 cells treated with copper nanoparticles (5&10µg/ml) for 6hr demonstrated a significant decrease in ROS production. This was deceptive that DCF light emission considering the quantity and quality in Fig. 7(A). Group I control doesn't exhibit much reactive oxygen species development. Group II depicts mild ROS production where it was treated with the copper nanoparticles of *Stachytarpheta cayennensis* (5µg/ml). At the same time, Group III illustrates elevated ROS formation where it was treated with the copper nanoparticles of *Stachytarpheta cayennensis* at (7.5µg/ml).

3.8 Outcome of *Stachytarpheta cayennensis* on mitochondrial membrane efficacy

Programmed cell death triggered by the modification of mitochondrial membrane potential was assessed by JC-1 staining dye (Fig. 7B). The control cells release increased light emission of green color, representing differentiated mitochondria membrane efficacy in Fig. 7B. Simultaneously, *Stachytarpheta cayennensis* copper nanoparticles (5µg/ml) established a noteworthy adjustment of ΔΨM, which

consistently abridged green color emission displays. Copper nanoparticles of *Stachytarpheta cayennensis* at about 7.5µg/ml were recognized notable in alteration of ΔΨM, which reliably exposed green color fluorescence.

3.9 Ethidium bromide and Acridine orange staining

The efficacy of Cu-NPs consequences in a different concentration-dependent manner in several viable cells well improved in late apoptotic and necrotic cells (Fig. 7C). The EB/AO staining assay is appropriate for copper nanoparticles in concurrence with the cell layer worsening viably. Control assemblage compared to untreated cells does not demonstrate any color variation. Group II treated with Cu-NP's of *Stachytarpheta cayennensis* (5µg/ml) showed a normalized number of viable cells. Simultaneously group III *Stachytarpheta cayennensis* Cu-NP's (7.5µg/ml) exhibited viable A375 cells with an increase in the number of early apoptotic cells.

3.10 Effect of copper nanoparticles of *Stachytarpheta cayennensis* on biochemical parameters

The results from Fig. 8 depict that SOD, CAT, GPx, and GSH activities were significantly diminished in DMBA only treated group II wherein TBARS was production augmented. At the same time group III mice treated with DMBA along with Cu-NP's of *Stachytarpheta cayennensis* (10 mg/kg bw) restored these enzymatic antioxidants levels. This was reversed with TBARS levels in which group III animals showed reduced TBARS. However, group IV animals exhibit no noteworthy decrease or increase in SOD, GSH, CAT, and GPx levels, similar to the control group I animals. Subsequently, TBARS also exhibited similar results.

3.11 Effect of copper nanoparticles on pro-inflammatory cytokines level

Figure 9 demonstrates that the levels of inflammatory markers were well improved by copper loaded *Stachytarpheta cayennensis*. It represents the effect of DMBA and copper nanoparticles of *Stachytarpheta cayennensis* (10 mg/kg bw) on pro-inflammatory cytokines IL-6, IL-1β, and TNF-α, levels. A significant augmentation in the planes of pro-inflammatory cytokines, TNF-α, IL-6, IL-1β altitudes was evident in the DMBA alone administered group (Group II). Whereas in group III, treatment of copper nanoparticles of Stachytarpheta and DMBA promisingly ($P < 0.05$) restored the levels of these inflammatory cytokines, which were comparable to the control group and the drug alone treated group IV animals.

3.12 Effect of Cu-NPs of Stachytarpheta on transcription signaling molecules of skin segments of control and experimental mice.

Figure 10 illustrates the levels of transcription signaling molecules, which were also amplified by copper loaded *Stachytarpheta cayennensis*. This signifies the effect of DMBA provoked and copper nanoparticles of *Stachytarpheta cayennensis* (10 mg/kg bw) on transcription molecules like NF-κB, COX-2, and iNOS, levels. An increase in the levels of COX-2, iNOS, and NF-κB planes was empirical in the DMBA only managed group (Group II). While in group III treatment with copper nanoparticles of

Stachytarpheta and DMBA ($p < 0.05$) reinstated the levels of these signaling molecules comparable to the control group and group IV mice.

3.13 Influence of copper loaded Stachytarpheta cayennensis on the lung histology of tissues

Figure 11 displays the histological inspection of the skin melanoma segment of control and experimental animals. Group I control mice exhibited standard architecture and slightly unaffected centers. Skin cancer holding or DMBA induced animals (group II) showed a tumoral structure with an asymmetrical architecture and bulky cells with dark nuclei and several minuscule hyper-refractile assemblies. Copper loaded *Stachytarpheta cayennensis* (10 mg/kg bw) along with DMBA induced group III animals unveiled recovered architecture, demonstrating the non-toxic feature of *Stachytarpheta cayennensis*. Pre-treatment with *Stachytarpheta cayennensis* alone (10 mg/kg bw) condensed the structural impairment in group IV animals, therefore, shielding the near usual architecture.

4. Discussion

For nanocrystals, the improved overlay of the electron and the wave functions in the space and narrowed structure augments the excited binding affinity, thus reflecting the excitonic peak probability, even at room temperature (Francois et al. 2019). In the present study, the UV absorption spectrum offers a qualitative suggestion of the size dispersal. That is, a sharp absorbance peak in the absorption spectrum in the case of small nanocrystals (Fig. 1) is undoubtedly an indication of the thin size dispersal of the nanoparticles of Stachytarpheta. This indication is verified in the ultraviolet-visible range using the surface plasmon resonance of copper nanoparticles. Current results were correlated with the preceding works (Mulvaney 1996). The FTIR spectra array of *Stachytarpheta cayennensis* established persistent shared peaks extending from 3266cm^{-1} to 660cm^{-1}. Figure 3 displays the expressive FTIR range attained from *Stachytarpheta cayennensis*. The occurrence originates from 3266cm^{-1}, which portrays the OH ranging signal, which shows amino acids and sugar molecules. The existence of 2909cm^{-1} peaks signify the hydrogen and carbon layer predominantly from a lipid molecule. The appearance of peaks from 1612cm^{-1} is the amide group (C = O) fluctuating due to protein degradation. The usage of metal-related nanoparticles is uninterruptedly mounting due to their extensive requests and exclusive physicochemical possessions. The cytotoxic efficacy of copper nanoparticles in various tumor cell lines was previously described (Ansilin et al. 2016; Thounaojam et al. 2011). We herewith state the role of copper nanoparticles synthesized from the *Stachytarpheta cayennensis* in human melanoma cells A375 and thereby analyzed its cytotoxic properties by MTT assay.

A few studies on the cytotoxicity of copper nanoparticles on different cell lines have been reported earlier (Midander et al. 2009). Preceding studies show the viability of CHO (Chinese hamster ovary) cells diminished to 25% at a 30µg/ml acquaintance of carbon-coated copper nanoparticles for 72hr, while the same treatment had no outcome on Hela cells (Studera et al. 2010). Most of the metal nanoparticles were described to induce intracellular ROS production (Sanpui et al. 2011; Wang et al. 2012; Siddiqui et al. 2013). In addition, a previous study illustrates that Cu-NP's increased the ROS level in human breast

cancer (MDA-MB-231) cells, which leads to cell death (Azizi et al., 2017). Consequently, the present study was designed to perceive whether Cu-NP generates ROS in A375 cells. In this case, the minimal ROS production in which cells were induced by the copper nanoparticles of *Stachytarpheta cayennensis* (5µg/ml). Moreover, group III mice show raised ROS production, which was induced by the copper nanoparticles of *Stachytarpheta cayennensis* at 7.5µg/ml. The electric charge distribution of the mitochondrial membrane was strongly connected to cell death. To examine whether Cu-NP's depolarized mitochondria of A375 cells, in the present study was executed. For this, A375 cells were treated with two different doses of Cu-NP (5µg/ml & 7.5µg/ml). The outcome showed that with increasing Cu-NP concentration, there was an increase in the mitochondrial membrane depolarization. The ultrastructural classification of Cu-NPs was conducted using TEM.

Though the Cu-NP's structure is proficient from TEM (200nm and 20 nm) it is slightly renowned than measurement considered using DLS (90 nm). This alteration on accretion was assigned to the diverse range of methods that provide irregular consequences in substance on the procedures that employ NP's (Sharma et al. 2009). Preceding studies determined the copper nanoparticles and copper concentrations distinguishingly disturbed the enzymatic antioxidants like CAT, SOD, and planes of TBARS in the mice serum (Rahmat et al. 2017). In the present study SOD, CAT, GPx, and GSH actions were downregulated in DMBA only treated group II. While group III mice, which were treated with DMBA as well as CuO NP's of *Stachytarpheta cayennensis* (10 mg/kg bw) reinstated these antioxidants levels. This was overturned in group III animals that displayed lowered levels of TBARS. Though, group IV animals revealed no notable decrease or upsurge in SOD, GSH, CAT, and GPx, which was comparable to control animals.

Previous work illustrates that melatonin could effectively mediate antitumor effect in melanoma cells by the diminished production of COX-2 and iNOS by regulating the nuclear translocation of NF-kB and retracting their binding affinity on COX-2 (Canhui et al. 2014). Likewise, in the current study, the inflammatory cytokines such as IL-6, IL-1β, and TNF-α and transcriptional signaling molecules like NF-kB, iNOS, and COX-2 were augmented in DMBA only treated group II animals. Treatment with copper nanoparticles of *Stachytarpheta cayennensis* (5µg/ml and 10µg/ml) showed downregulated expression of the aforementioned signaling molecules in a concentration-dependent manner wherein 10µg/ml of Cu-NPs exhibited lowered expressions. Thus, copper loaded *Stachytarpheta cayennensis* management restored these markers' levels comparable to normal, suggesting its anticancer effect over skin melanoma cancer.

5. Conclusion

The current study of Cu-NP's synthesis was carried out using the plant extract of *Stachytarpheta cayennensis* followed by characterization using UV-Visible spectroscopy, dynamic light scattering, and FTIR. Further, we assessed the anti-melanoma efficiency of biosynthesized copper nanoparticles from *Stachytarpheta cayennensis*. The consequences propose that Cu-NPs induced cytotoxicity through a ROS generation and membrane potential. Cell viability assays and adhesion assay was carried out in a concentration-dependent manner. Pro-inflammatory marker and cytokine levels were also estimated to

confirm the efficacy of *Stachytarpheta cayennensis*. Molecular mechanisms of cellular transcription molecules were done by RT-PCR studies. Ultimately we propose that biosynthesized copper nanoparticles from *Stachytarpheta cayennensis* might be an excellent choice to treat skin melanoma cancer.

Declarations

Acknowledgment:

The authors would like to thank the Deanship of Scientific Research, Prince Sattam bin Abdul Aziz University, Al- Kharj, Kingdom of Saudi Arabia for their support.

Data Availability

The data used to support the findings of this study are available from the corresponding author upon request.

Conflicts of Interest:

The authors declare no conflicts of interest

References

1. Adebajo, A.C., Olawode, O.R., Adesanya, S.A., Begrow, F., Elkhawad, A., Akanmum, R., Edrada, M., AProksh, P. and Scmidt, T.J. (2007) Hypoglycemic Constituent of Stachytarpheta cayennensis Leaf. Planta Medica, 73, 241-250.
2. Akintelu SA, Folorunso AS, Folorunso FA, Oyebamiji AK. Green synthesis of copper oxide nanoparticles for biomedical application and environmental remediation. Heliyon. 2020; 6(7): e04508.
3. Attalla F. El-Kott. Anti-Angiogenic Effectiveness of the Pomegranate Against Benzo(a)Pyrene Induced Lung Carcinoma in Mice. International Journal of Cancer Research 11 (4): 164-174, 2015.
4. Azizi M, Ghourchian H, Yazdian F, Dashtestani F, Zeinabad HA. Cytotoxic effect of albumin coated copper nanoparticles on human breast cancer cells of MDA-MB-231. PLoS One. 2017; 12(11): e0188636.
5. Canhui Yi, Yong Zhang, Zhenlong Yu, Yao Xiao, Jingshu Wang, Huijuan Qiu, Wendan Yu, Ranran Tang, Yuhui Yuan, Wei Guo, Wuguo Deng. (2014) MelatonCu-NP'sces the Anti-Tumor Effect of Fisetin by Inhibiting COX-2/iNOS and NF-kB/p300 Signaling Pathways. PLoS ONE 9(7): e99943. doi:10.1371/journal.pone.0099943.
6. Deborah Ribble, Nathaniel B Goldstein, David A Norris and Yiqun G Shellman. A simple technique for quantifying apoptosis in 96-well plates. BMC Biotechnology 2005, 5:12.
7. Francois Eya'ane Meva1, Joel Olivier Avom Mbeng, Cecile Okalla Ebongue, Carsten Schlüsener, Ülkü Kökçam-Demir, Agnes Antoinette Ntoumba, Phillipe Belle Ebanda Kedi, Etienne Elanga, Evrard-Rudy

Njike Loudang, Moise Henri Julien Nko' o, Edmond Tchoumbi, Vandi Deli, Christian Chick Nanga, Emmanuel Albert Mpondo Mpondo, Christoph Janiak. Stachytarpheta cayennensis Aqueous Extract, a New Bioreactor towards Silver Nanoparticles for Biomedical Applications. Journal of Biomaterials and Nanobiotechnology, 2019, 10, 102-119.

8. Goth L. A simple method for determination of serum catalase activity and revision of reference range. Clin Chim Acta. 1991;196(2):143-51.
9. Gunaseelan, S., Balupillai, A., Govindasamy, K. et al. 2017. Linalool prevents oxidative stress activated protein kinases in single UVB-exposed human skin cells. PLoS One .12(5): e0176699.
10. Hongfeng Wu Zhongtao Li, Jiaoqing Tang, Xiao Yang, Yong Zhou, Bo Guo, Lin Wang, Xiangdong Zhu, Chongqi Tu, Xingdong Zhang. The in vitro and in vivo anti-melanoma effects of hydroxyapatite nanoparticles: influences of material factors. International Journal of Nanomedicine 2019:14 1177–1191.
11. Laha D, Pramanik A, Maity J, Mukherjee A, Pramanik P, Laskar A and Karmakar P 2014 Interplay between autophagy and apoptosis mediated by copper oxide nanoparticles in human breast cancer cells MCF7 Biochimica et Biophysica Acta 1840 1–9 doi.org/10.1016/j.bbagen.2013.08.011.
12. Li S, Liu J, Sun M, Wang J, Wang C, Sun Y. Cell membrane-camouflaged nanocarriers for cancer diagnostic and therapeutic. Front Pharmacol. 2020; 11: 24.
13. M.C. Thounaojam, R.N. Jadeja, M. Valodkar, P.S. Nagar, R.V. Devkar, S. Thakore, Oxidative stress induced apoptosis of human lung carcinoma (A549) cells by a novel copper nanorod formulation, Food Chem. Toxicol. 49 (11) (2011) 2990–2996.
14. Melvin Joe, M., Jayochitra, J. & Vijayapriaya, M. (2009). Antimicrobial activity of some common spices against certain human pathogens. J. Med. Plants Res, 3, 1134-1136.
15. Metz, K.M., Sanders, S.E., Pender, J.P., Dix, M.R., Hinds, D.T., Quinn, S.J., Ward,A.D., Duffy, P., Cullen, R.J. and Colavita, P.E. (2Nko' Green Synthesis of Metal Nanoparticles via Natural Extracts: The Biogenic Nanoparticle Corona and Its Effects on Reactivity. ACS Sustainable Chemistry and Engineering, 3, 1610-1617.
16. Meva, F. E., Segnou, M.L., Ebongue, C.O., Ntoumba, A.A., Steve, D.Y., Malolo, F. E.A., Ngah, L., Massai, H. and Mpondo, E.M. (2016) Unexplored Vegetal for the Green Synthesis of Silver Nanoparticles: A Preliminary Study with Corchorus olitorus Linn and Ipomoea batas (L.) Lam. African Journal of Biotechnology, 15, 341-349.
17. Midander K, Cronholm P, Karlsson H L, Elihn K, Mo¨ller L, Leygraf C and Wallinder I O 2009 Surface Characteristics, Copper Release, and Toxicity of Nano- and Micrometer-Sized Copper and Copper(II) Oxide Particles: A Cross-Disciplinary Study small 5 389–399 doi: 10.1002/smll.200801220.
18. Miller R, Walker S, Shui I, Brandtmuller A, Cadwell K, Scherrer E. Epidemiology and survival outcomes in stages II and III cutaneous melanoma: a systemic review. Melanoma Manag. 2020; 7(1): MMT39. doi: 10.2217/mmt-2019-0022.
19. Mosmann T 1983 Rapid colorimetric assay for cellular growth and survival: application to proliferation and cytotoxicity assays J. Immunol.Methods 65 55-63.

20. Mulvaney, P. (1996) Surface Plasmon Spectroscopy of Nanosized Metal Particles. Langmuir, 12, 788-800.
21. Okoye TC, Akah PA, Okoli CO, Ezike AC, Mbaoji FN. Antimicrobial and antispasmodic activity of leaf extract and fractions of *Stachytarpheta cayennensis*. Asian Pacific J Tropical Med. 2010; 3(3): 189-192.
22. Okoye, T.C., Akah, P.A., Okoli, C.O., Ezike, A.C. and Mbaoji, F.N. (2010) Antimicrobial and Antispasmodic Activity of Leaf Extract and Fractions of Stachytarpheta cayennensis . Asian Pacific Journal of Tropical Medicine, 3, 189-192.
23. Panido C, Costa KA, Futuro DO, Paiva SR, Kaplan MAC, Figueiredo MR, Henriques MGMO. Anti-inflammatory and anti-ulcerogenic properties of *Stachytarpheta cayennensis* (L.C. Rich) Vahl. J Ethnopharmacol. 2006: 104(1-2): 225-233.
24. Patra M, Roy S S, Dasgupta R and Basu T 2015 GroEL to DnaK Chaperone Network behind the Stability Modulation of σ32 at Physiological Temperature in Escherichia coli. FEBS Letters 589 4047-4052.
25. Rahmat-Allah Fatahian-Dehkordi, Mahbobe Reaisi, Mohamad-Saeed Heidarnejad, Abdonnaser Mohebbi. Serum biochemical status and morphological changes in mice ovary associated with copper oxide nanoparticles after thiamine therapy. J Herb med Pharmacol. 2017; 6(1): 21-26.
26. Ria Mukhopadhyay, Julekha Kazi, Mita Chatterjee Debnath. Synthesis and characterization of copper nanoparticles stabilized with Quisqualis indica extract: Evaluation of its cytotoxicity and apoptosis in B16F10 melanoma cells. Biomedicine & Pharmacotherapy 97 (2018) 1373–1385.
27. Ruan JS, Liu YP, Zhang L, Yan LG, Fan FT, Shen CS, Wang AY, Zheng SZ, Wang SM, Lu Y. Luteolin reduces the invasive potential of malignant melanoma cells by targeting beta- 3-integrin and the epithelial-mesenchymal transition. Acta Pharmacologica Sinica 2012; 33: 1325-1331.
28. Ansilin, J.K. Nair, C. Aswathy, V. Rama, J. Peter, J.J. Persis, Green synthesis and characterisation of copper oxide nanoparticles using Azadirachta indica (Neem) leaf aqueous extract, J. Nanosci. Tech. 2 (5) (2016) 221–223.
29. Sanchez-Lopez E, Gomes D, Esteruelas G, Bonilla L, Lopez-Machado AL, Galindo R, Cano A, Espina M, Ettcheto M, Camins A, Silva AM, Durazzo A, Santini A, Garcia ML, Souto EB. Metal-based nanoparticles as antimicrobial agents: an overview. Nanomaterials (Basel). 2020; 10(2): 292.
30. Schapoval, E.E.S., De Vargas, W.M.R., Chaves, C.G., Bridi, R., Zuanazzi, J.A. and Henriques, A.T. (1998) Antiinflammatory and Antinociceptive Activities of Extracts and Isolated Compounds from Stachytarpheta cayennensis . Journal of Ethnopharmacology, 60, 53-59.
31. Shi J., Peng C., Yang Y., Yang J., Zhang H., Yuan X., Chen Y., Hu T. Phytotoxicity and accumulation of copper oxide nanoparticles to the Cu-tolerant plant *Elsholtzia splendens*. Nanotoxicology. 2014;8:179–188. doi: 10.3109/17435390.2013.766768.
32. Siddiqui M A, Alhadlaq H A, Ahmad J, Al-Khedhairy A A, Musarrat J and Ahamed M 2013 Copper Oxide Nanoparticles Induced Mitochondria Mediated Apoptosis in Human Hepatocarcinoma Cells. PLoS ONE 8 doi: 10.1371/journal.pone.0069534.

33. Siddiqui M A, Alhadlaq H A, Ahmad J, Al-Khedhairy A A, Musarrat J and Ahamed M 2013 Copper Oxide Nanoparticles Induced Mitochondria Mediated Apoptosis in Human Hepatocarcinoma Cells. PLoS ONE 8 doi: 10.1371/journal.pone.0069534.
34. Silva, L.P., Reis, I.G. and Bonatto, C.C. (2015) Green Synthesis of Metal Nanoparticles by Plants: Current Trends and Challenges. In: Basiuk, V.Eya'anesiuk, E., Eds.,Green Processes for Nanotechnology , Springer, Cham, 259-275.
35. Srilatha Sakamuru, Matias S. Attene-Ramos, and Menghang Xia. Mitochondrial Membrane Potential Assay. Methods Mol Biol. 2016; 1473: 17–22.
36. Studera A M, Limbach L K, Duc L V, Krumeich F, Athanassiou E K, Gerber L C, Moch H and Stark W J 2010 Nanoparticle cytotoxicity depends on intracellular solubility:Comparison of stabilized copper metal and degradable copper oxide nanoparticles Toxicology Letters 197 169–174 doi:10.1016/j.toxlet.2010.05.012.
37. Sun T, Yan Y, Zhao Y, Guo F and Jiang C 2012 Copper Oxide Nanoparticles Induce Autophagic Cell Death in A549 Cells PLoS ONE 7 doi: 10.1371/journal.pone.0043442.
38. Sun T, Yan Y, Zhao Y, Guo F, Jiang C. Copper oxide nanoparticles induce autophagic cell death in A549 cells. PLoS One. 2012;7(8): e43442.
39. Tomic T, Botton T, Cerezo M, et al. metformin inhibits melanoma development through autophagy and apoptosis mechanisms. Cell Death Dis. 2011;2(9): e199.
40. Sharma, R.K. Shukla, N. Saxena, D. Parmar, M. Das, A. Dhawan, A, DNA damaging potential of zinc oxide nanoparticles in human epidermal cells, ToCu-NP'sett. 185 (3) (2009) 211–218.
41. Wang Y, Yang F, Zhang H X, Zi X Y, Pan X H, Chem F, Luo W D, Li J X, Zhu H Y and Hu Y P 2013 Cuprous oxide nanoparticles inhibit the growth and metastasis of melanoma by targeting mitochondria Cell Death Dis. 4 doi:10.1038/cddis.2013.314.
42. Wang Z, Li N, Zhao J, White J C, Qu P and Xing B 2012 CuO Nanoparticle Interaction with Human Epithelial Cells: Cellular Uptake, Location, Export, and Genotoxicity Chem. Res. Toxicol. 25 1512−1521.
43. Yaqub, A., Malkani, N., Shabbir, A. et al. Novel biosynthesis of copper nanoparticles using *Zingiber* and *Allium* sp. with synergic effect of doxycycline for anticancer and bactericidal activity. Curr Microbiol. 2020; 77: 2287–2299. https://doi.org/10.1007/s00284-020-02058-4.
44. Zottel A, Paska AV, Jovcevska I. Nanotechnology meets oncology: nanomaterials in brain cancer research, diagnosis and therapy. Materials (Basel). 2019; 12(10): 1588.

Figures

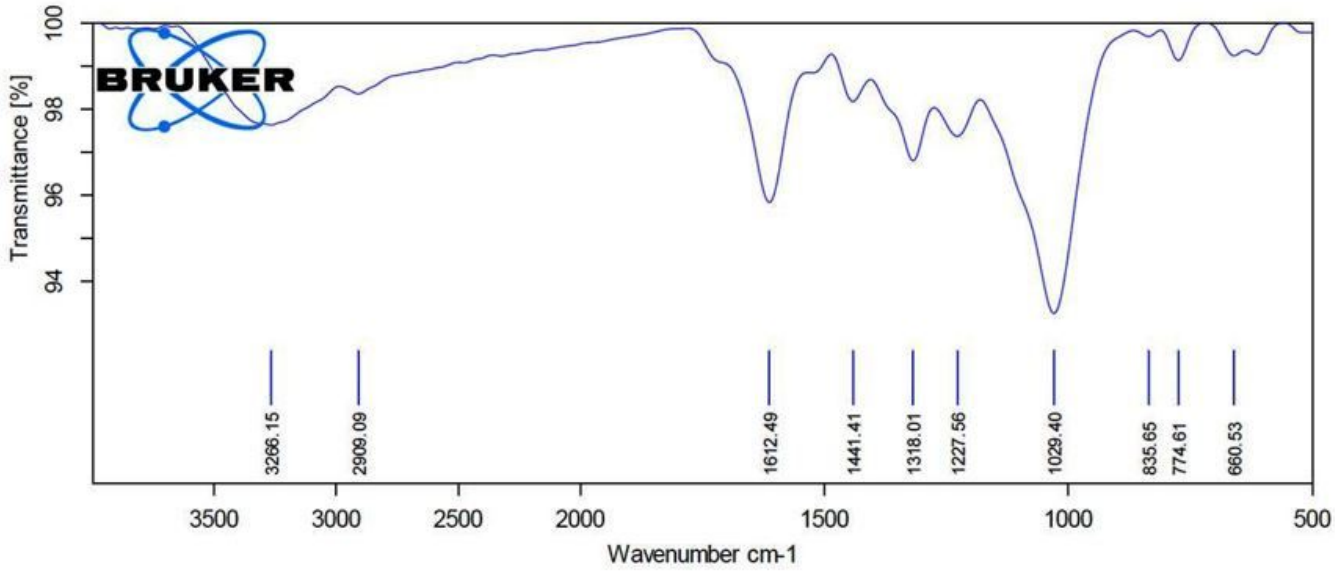

Stachytarpheta cayennensis were liable for the association and formation of nanoparticles. The FTIR range of *Stachytarpheta cayennensis* established abundant absorption ranges varied from 3266cm^{-1} to 660cm^{-1}.

Figure 3

FTIR spectrum of copper loaded Stachytarpheta cayennensis

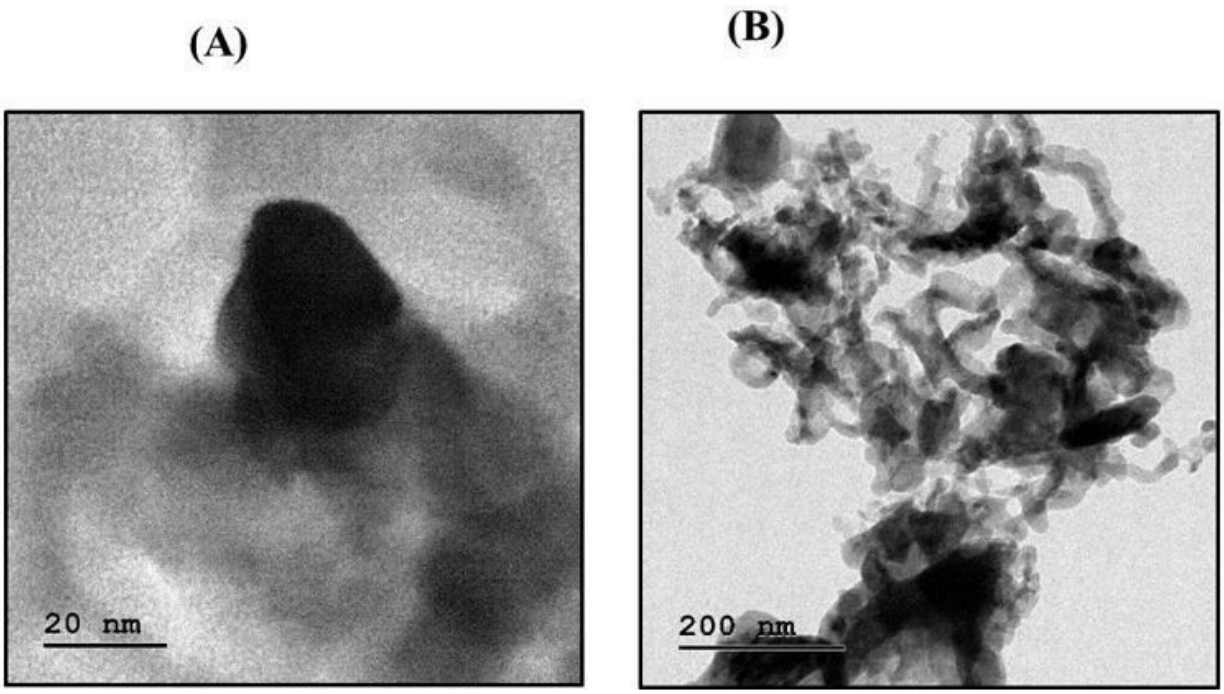

TEM images exhibited that the synthesized Cu-NPs irregular structures with the size ranging from 30-100nm.

Figure 4

Transmission electron microscopy analysis of synthesized Cu-NPs

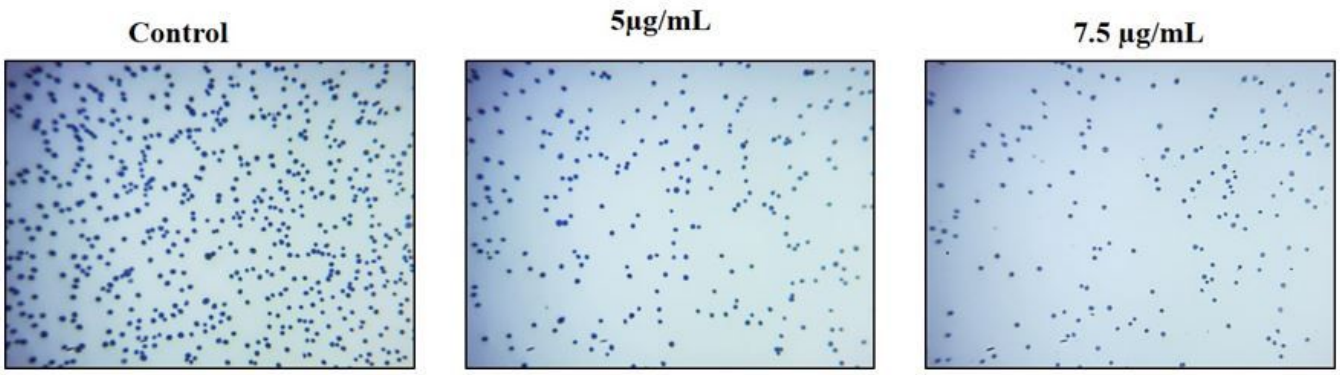

Cell adhesion examination Staining with 0.1% crystal violet (intensification × 100) exposed abridged bond in cells articulating in 12hr in all three groups, control, *Stachytarpheta cayennensis* and normal; whereas at 24hr 7.5µg/mL handling of *Stachytarpheta cayennensis* uncovered attached cells which was equivalent to the control cells.

Figure 6

Cell adhesion assay